NEUROSCIENCE
RESEARCH PAPER
J. Carcaud et al. / Neuroscience 374 (2018) 33–48

Differential Processing by Two Olfactory Subsystems in the Honeybee Brain

Julie Carcaud, [a,b] **Martin Giurfa** [b] **and Jean-Christophe Sandoz** [a]*

[a] *Evolution, Genomes, Behavior and Ecology, CNRS, Univ Paris-Sud, IRD, Université Paris Saclay, 1 avenue de la Terrasse, 91198 Gif-sur-Yvette, France*

[b] *Centre de Recherches sur la Cognition Animale, Centre de Biologie Intégrative (CBI), Université de Toulouse, CNRS, UPS, 31062 Toulouse Cedex 9, France*

Abstract—Among insects, Hymenoptera present a striking olfactory system with a clear neural dichotomy from the periphery to higher order centers, based on two main tracts of second-order (projection) neurons: the medial and lateral antennal lobe tracts (m-ALT and l-ALT). Despite substantial work on this dual pathway, its exact function is yet unclear. Here, we ask how attributes of odor quality and odor quantity are represented in the projection neurons (PNs) of the two pathways. Using *in vivo* calcium imaging, we compared the responses of m-ALT and l-ALT PNs of the honey bee *Apis mellifera* to a panel of 16 aliphatic odorants, and to three chosen odorants at eight concentrations. The results show that each pathway conveys differential information about odorants' chemical features or concentration to higher order centers. While the l-ALT primarily conveys information about odorants' chain length, the m-ALT informs about odorants' functional group. Furthermore, each tract can only predict chemical distances or bees' behavioral responses for odorants that differ according to its main feature, chain length or functional group. Generally l-ALT neurons displayed more graded dose–response relationships than m-ALT neurons, with a correspondingly smoother progression of inter-odor distances with increasing concentration. Comparison of these results with previous data recorded at AL input reveals differential processing by local networks within the two pathways. These results support the existence of parallel processing of odorant features in the insect brain.

Key words: insect, antennal lobe, parallel processing, projection neurons, optical imaging.

INTRODUCTION

Olfaction provides animals with crucial information in a variety of behavioral contexts that are common across species, like mating, feeding or detecting danger. The anatomical architecture of the olfactory system shows, therefore, a remarkable interspecific similarity (Hildebrand and Shepherd, 1997; Ache and Young, 2005). The primary olfactory center (the olfactory bulb in vertebrates, the antennal lobe (AL) in insects and the olfactory lobe in crustaceans) is composed of numerous functional units termed glomeruli (Pinching and Powell, 1971; Hansson and Anton, 2000). Each glomerulus receives input from many olfactory receptor neurons (ORNs) expressing one type of olfactory receptor (Gao et al., 2000; Vosshall, 2000; Imai and Sakano, 2007). Local, mostly inhibitory, interneurons interconnect glomeruli and thus reshape the olfactory message (Puopolo and Belluzzi, 1998; Seki et al., 2010; Grabe et al., 2016; Nagel and Wilson, 2016). This local processing involves both a gain control that avoids saturation of the signal and asymmetrical inhibition qualitatively reshaping the olfactory representation (Tabor et al., 2004; Bhandawat et al., 2007; Deisig et al., 2010; Adam et al., 2014; Kim et al., 2015). The olfactory message is then conveyed to higher olfactory centers by mitral/tufted cells in vertebrates, or by projection neurons (PNs) in insects (Haberly and Price, 1977; Kanzaki et al., 1989). These neurons usually project to several brain centers, such as the amygdala and the piriform cortex in vertebrates (Mori and Sakano, 2011; Igarashi et al., 2012), or the lateral horn and the mushroom bodies in insects (Laurent, 2002; Tanaka et al., 2004; Kirschner et al., 2006).

Parallel processing is defined as the coding and processing of different features of the same stimulus by distinct neural pathways and has been demonstrated in several sensory modalities in both insects and vertebrates (Rauschecker and Tian, 2000; Yamaguchi et al., 2008; Nassi and Callaway, 2009). As it is ubiquitous in neural systems, it may represent an adaptive strategy

*Correspondence to: J.-C. Sandoz, Evolution, Genomes, Behavior and Ecology, CNRS, Univ Paris-Sud, IRD, Université Paris Saclay, 1 avenue de la Terrasse, 91198 Gif-sur-Yvette, France.
E-mail address: sandoz@egce.cnrs-gif.fr (J.-C. Sandoz).

https://doi.org/10.1016/j.neuroscience.2018.01.029
0306-4522/

for living organisms, ensuring more efficient and rapid processing of inherently complex sensory stimuli. Olfactory systems are especially interesting for the study of parallel processing because within the general architecture detailed above, they harbor several distinct pathways in which the reshaping of odor information may differ (Galizia and Rössler, 2010; Rössler and Brill, 2013). Among insects, this is particularly true in Hymenoptera like the honey bee, which exhibit an olfactory system with multiple PN tracts: the median (m-ALT), the lateral (l-ALT) and three smaller medio-lateral tracts (ml-ALTs) (Abel et al., 2001; Müller et al., 2002; Kirschner et al., 2006; Galizia and Rössler, 2010; Zwaka et al., 2016). The m-ALT and l-ALT are particularly remarkable as they are of almost equal size in terms of neuron numbers (~400 vs ~500) (Rybak, 2012) and project both to the mushroom bodies and the lateral horn, but in reverse order. As each PN type collects information from segregated subsets of AL glomeruli, m-ALT and l-ALT may be envisaged as forming part of two different subsystems. Here we will adopt the term *m-subsystem* to define the olfactory pathway proper to m-ALT PNs, starting at the receptor level and finishing at the PNs themselves. In the same way, we will adopt the term *l-subsystem* for the olfactory pathway corresponding to l-ALT PNs, from the receptor level to the PNs. These subsystems have been the focus of numerous neuroanatomical and neurophysiological studies, which reported differences in odor specificity, response latency, concentration dependence or coincident activity (Müller et al., 2002; Krofczik et al., 2009; Yamagata et al., 2009; Brill et al., 2013, 2015; Carcaud et al., 2015). Yet, if and how different chemical features of odorants are processed within each subsystem and if the reshaping of the odor message imposed by local AL networks differs between the two subsystems remains largely unknown.

We addressed these questions in the honey bee by recording via *in vivo* calcium imaging the activity of m-ALT and l-ALT PNs to a standard panel of aliphatic odorants differing in two chemical features (functional group and carbon chain length) or in their concentration (Fig. 1A). We then compared PN responses to our previous recordings of AL activity dominated by ORN signals and provided a fair approximation to AL input activity (Carcaud et al., 2012). Our results show that the reshaping of local odor information within the AL network differentially affects the two subsystems, with a more significant reshaping occurring in the m-subsystem. Our data also reveal that each PN type conveys different, but complementary, information about odorants to higher order centers.

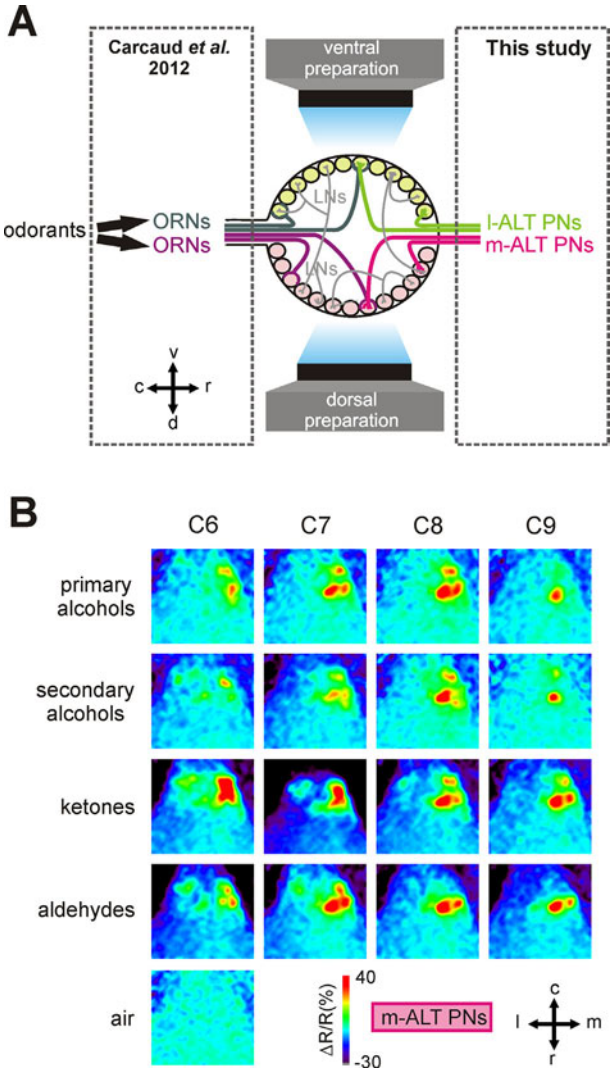

Fig. 1. Calcium signals from m- and l-ALT PNs in the AL. (A) Schematic drawing of the AL network. Odorants molecules are detected by ORNs on the antenna, which send olfactory information to the antennal lobe. ORNs convey their information either in the ventral surface of the AL (l-subsystem, light green) or in the dorsal surface of the AL (m-subsystem, light pink). Within the AL, local neurons (LNs, gray) interconnect glomeruli. Then, projection neurons (PNs) convey information to higher brain centers, the mushroom bodies and the lateral horn, through two main tracts of PNs, the m-ALT (magenta) and l-ALT (green). Responses of PNs were recorded in the present study, from both AL subsystems. Data were compared to ORN responses recorded in a previous study (Carcaud et al., 2012). (B) Odor-induced calcium signals in glomeruli innervated by m-ALT PNs, to a panel of 16 aliphatic odorants varying according to their chemical functional group (primary and secondary alcohols, aldehydes and ketones) and their carbon chain length (C6–C9). Relative ratio changes ($\Delta R/R\%$) are presented in a false-color code, from dark blue to red. Different odors induce different glomerular activity patterns in glomeruli innervated by m-ALT PNs. c: caudal, r: rostral, v: ventral, d: dorsal, l: lateral, m: medial. (For interpretation of the references to color in this figure legend, the reader is referred to the web version of this article.)

EXPERIMENTAL PROCEDURES

Animals

Honeybee workers (*Apis mellifera* females) were collected at the entrance of an outdoor hive. They were chilled on ice until they stopped moving, and were then placed in recording chambers using low temperature melting wax. Different animals were used to record l-ALT and m-ALT PNs since visualizing each subsystem requires a different preparation. To record activity from glomeruli innervated by the l-ALT PNs, we employed the standard imaging preparation used in prior studies (Joerges et al., 1997; Sachse and Galizia, 2002); briefly,

a window was cut into the cuticle of the head between the compound eyes, the ocelli and the antennal bases. Salivary glands and trachea sacks were then gently removed, thereby access the two ALs. A different preparation was used to visualize the glomeruli innervated by the m-ALT (Carcaud et al., 2015). Honeybees were fixed on their back on a plastic chamber, and their antennae were inserted into a small slit, so that odor presentations could be applied from below the chamber (Carcaud et al., 2012, 2015). As in the other preparation, the cuticle was cut open and the tentorial arms, glands and trachea were carefully removed to expose the brain. In both preparations, the brain was immersed in saline solution (in mM: NaCl, 130; KCl, 6; $MgCl_2$, 4; $CaCl_2$, 5; sucrose, 160; glucose, 25; HEPES, 10; pH 6.7, 500 mOsmol; all chemicals from Sigma-Aldrich, Lyon, France). PNs were stained using a glass electrode coated with the calcium indicator Fura-2 dextran (potassium salt, 10,000 kDa, in 2% BSA; Life technologies, France) mixed with tetramethylrhodamine dextran (10,000 kDa; Life technologies, France) (Sachse and Galizia, 2002; Yamagata et al., 2009). To stain l-ALT neurons, the electrode was inserted in their axonal path, between the α lobe and the border of the optic lobe, rostrally from the lateral horn. To stain m-ALT neurons, the electrode was inserted in their axonal path, in the medial part of the protocerebrum, rostrally from the AL. In both cases, the dyes migrated retrogradely toward the AL thereby staining glomeruli that were innervated either by m-ALT or by l-ALT PNs. The bee was then left in a humid and dark box for at least 3 h. After calcium imaging recordings, a neuroanatomical step (see below) checked for efficient and homogeneous staining of each type of PN tract.

Optical recordings and odor stimulation

Calcium imaging measurements were performed in standard conditions (Mota et al., 2013; Carcaud et al., 2015), using a T.I.L.L. Photonics imaging setup (Martinsried, Germany). Stained bees were placed under the 10× water-immersion objective (Olympus, UMPlanFL; NA 0.3) of an epifluorescent microscope (Olympus BX-51WI). Recordings were performed using a 640 × 480 pixel 12-bit monochrome CCD-camera (T.I.L.L), with 4 × 4 binning on chip (pixel image size: 4.8 μm × 4.8 μm). Excitation alternated between 340 nm and 380 nm monochromatic light (T.I.L.L. Polychrom IV). Each measurement comprised 100 double frames applied at a frequency of 5 Hz. Fluorescence was detected with a 490 nm dichroic filter and a bandpass 525/50 nm emission filter. Integration time was 4–20 ms at 380 nm excitation and 16–80 ms at 340 nm excitation. Olfactory stimulation lasted for 1 s, starting at the 15th frame and lasting until the 20th frame.

Two separate experiments were conducted. One experiment studied the coding of odor quality, while the other focused on the coding of odor quantity. In order to assess the activity of AL networks (i.e., local interneurons) in both subsystems, we used the same odorants of our previous study which recorded a signal emphasizing ORN activity, i.e., the input to the AL (Carcaud et al., 2012). For the odor quality experiment, we thus used 16 aliphatic odorants belonging to four functional group types (primary and secondary alcohols, aldehydes and ketones) and carrying four different carbon chain lengths (6, 7, 8 and 9 carbons). Bees received up to three runs, each comprising all stimuli presented in a randomized order. In the odor quantity experiment, we used three odorants (1-hexanol, heptanal and 2-octanone) at eight different concentrations. Odor concentration was varied by diluting pure odor substance in mineral oil, resulting in different effective amounts on the filter paper (from 10^{-7} to 10^{0}, i.e., pure). Odorants were presented in increasing concentration order, from 10^{-7} to 10^{0}, to limit adaptation. Here too, bees received up to three runs with all stimuli. Odor solutions (5 μL, Sigma–Aldrich, France), either pure (first experiment) or diluted in mineral oil (second experiment), were applied onto 1 cm^2 pieces of filter paper and placed into Pasteur pipettes. A pipette containing a clean piece of filter paper (experiment 1) or soaked with mineral oil (5 μL, experiment 2) was used as control stimulus. In both experiments, a constant clean airstream into which odor pulses of controlled duration could be introduced was sent to the bees' antennae by an olfactometer placed at a distance of 2 cm to the bee. The interval between odor presentations was ~80 s. Only bees that experienced at least one complete run of odor stimulations were kept for the analyses.

Anatomical staining

After optical imaging recordings, the brains were dissected and fixed in 4% formaldehyde in PBS overnight at 4 °C. The next day, they were washed in PBS and then dehydrated in standard ethanol series. Finally, they were cleared in methyl salicylate (Sigma–Aldrich, Deisenhofen, Germany). Each AL was then visualized with a confocal laser-scanning microscope (Zeiss LSM 700, 555 nm excitation wavelength) and a water immersion objective (20× plan-apochromat 1.0NA, Zeiss, Jena, Germany).

Data processing

Optical imaging data were analyzed using custom software in IDL 6.0 (Research Systems Inc., Colorado, USA). Each recording corresponded to a 4-dimensional array with the excitation wavelength (340 nm or 380 nm), two spatial dimensions (x, y pixels of the area of interest) and the temporal dimension (100 frames). Data analysis was performed in three steps following Galizia and Vetter (2004). First, the ratio $R = F_{340\ nm}/F_{380\ nm}$ was calculated at each pixel and time point. Relative ratio changes were then computed as $\Delta R/R = (R - R_0)/R_0$, with the average of five frames before the start of any olfactory stimulation (frames 10–14) as reference R_0. To reduce the effects of photon and electronic noise, these data were filtered in both spatial dimensions and in the temporal dimension using a three pixel median filter. Third, a bleach correction was applied. For each recording, a logarithmic curve fitted to the median brightness decay of the entire image frames, excluding the frames during the stimulus until 5 s after stimulus onset, was sub-

tracted from the data (Galizia and Vetter, 2004). Such a correction stabilizes the baseline of the recordings without affecting odor-evoked responses.

Intensity and similarity measure

Odor-response maps could then be calculated. For each odor stimulation of each animal, the map contains the amplitude of the calcium response of each pixel, calculated as the mean of three frames during the stimulus (frames 17–19) minus the mean of three frames before odor presentation (frames 12–14). For better visualization of activity spots, odor-response maps were subjected to a 7×7 Gaussian filter and presented in the figures following a false color code from dark blue to red. For data analysis, the different maps obtained for each odor (1–3 runs) within each individual bee were averaged. For each bee, a mask was manually drawn around the AL in order to remove all regions that did not correspond to the AL from the analysis. This ensured the comprehensive analysis of all glomerular activity on each AL (Carcaud et al., 2012, 2015).

To calculate the *intensity* of each odor-evoked response, the intensity ($\Delta R/R$ in %) of all pixels located within the unmasked area of the AL were averaged. To evaluate the *similarity* among neural representations, pixelwise Euclidean distances (a measure of dissimilarity) were calculated for all odor pairs, according to the following standard equation:

$$d_{ij} = \sqrt{\sum_{k=1}^{p} (X_{ik} - X_{jk})^2}$$

In this equation, i and j indicate odorants, p the number of pixels in unmasked area of the AL, and X_{ik} represents the amplitude of the response in pixel k to odor i.

Statistical analysis

The intensities of responses to the different odors were compared using ANOVA for repeated measurements. When significant, Dunnett's test was applied to compare the intensity of each odor response to a common reference, either the air control (experiment 1) or the solvent control (mineral oil, experiment 2). ANOVA for repeated measurements was also used to compare intensities depending on functional group and carbon chain length or to compare Euclidian distances depending on differences in the length of the carbon chain, and a Tukey test was applied as post hoc test. Wilcoxon matched-pairs tests were applied to compare Euclidian distances between odors with the same or with a different functional group (or chain length).

To ask how response maps recorded in l-ALT and in m-ALT PNs related to chemical distances between odorant molecules (Haddad et al., 2008) or to evaluate if they could predict bees' generalization behavior (Guerrieri et al., 2005), we used multiple regressions analyses. In both cases, a common model with two explanatory variables (l-ALT distances, m-ALT distances) plus their possible interaction was used, assessing the significant participation of each variable or interaction.

Pearson correlation analyses were performed between response intensities in m- or l-ALT neurons and odorant vapor pressure, or between response intensities or Euclidian distances measured at the input and output in both subsystems. Mantel tests were used to test whether correlations between Euclidian distances measured at the input and output were significant.

ANOVA for repeated measurements were also used to compare odor-evoked intensities or distances between odors depending on the concentration, both in the m-ALT and in the l-ALT PNs. Tukey test was applied as post hoc test. All tests were performed with Statistica 7.1 or *R* (www.r-project.org).

RESULTS

We performed *in vivo* calcium imaging of the AL after injection of Fura-2 dextran in either l-ALT PNs, using the standard ventral preparation, or in m-ALT PNs, using the recently developed dorsal preparation (Carcaud et al., 2015). We therefore compared odor-coding properties in both PN types at the level of their dendrites within the glomeruli (Fig. 1A). Honey bees were stimulated with the same odorants used in a previous study, which recorded a compound signal dominated by ORN activity and which thus constitutes a fair approximation of input signals into the AL (Carcaud et al., 2012). The use of the same odorants enables the comparison of odor-coding rules at the input and output levels of the AL, and allows determining the net effect of local processing by AL networks in both the m- and the l-subsystems.

Transformation of odor quality information

We explored the coding of odor quality at the output of the AL, i.e., at the level of both PN pathways. Sixteen aliphatic odorants were used to this end, which differed in their functional group (primary and secondary alcohols, aldehydes and ketones) and in their carbon chain length (C6, C7, C8 and C9). All odorants induced clear activity patterns in both m-ALT neurons ($n = 9$, Fig. 1B) and l-ALT neurons ($n = 10$), with different odorants activating different combinations of glomeruli. We first compared response intensity and similarity relationships among activity maps in the two PN pathways as a function of odorant chemical features such as carbon chain length and functional group.

Response intensity of PNs. All 16 odorants induced significant activity in comparison to the air control, both in m- and l-ALT PNs (Fig. 2A, all odors $p < 0.01$, post hoc Dunnett tests). Overall, response intensity was similar in m-ALT and l-ALT neurons (*PN type* effect, $F_{1,17} = 2.27$, NS), but the two PN types responded differently to the 16 odorants (*odor* $\times$ *PN type* interaction, $F_{15,255} = 1.8$, $p < 0.05$). Both m-ALT and l-ALT neurons showed different responses depending on the odorants' functional group (Fig. 2B upper panel, *functional group* ANOVA, m-ALT: $F_{3,24} = 19.7$, $p < 0.001$; l-ALT: $F_{3,27} = 11.6$, $p < 0.001$). In m-ALT

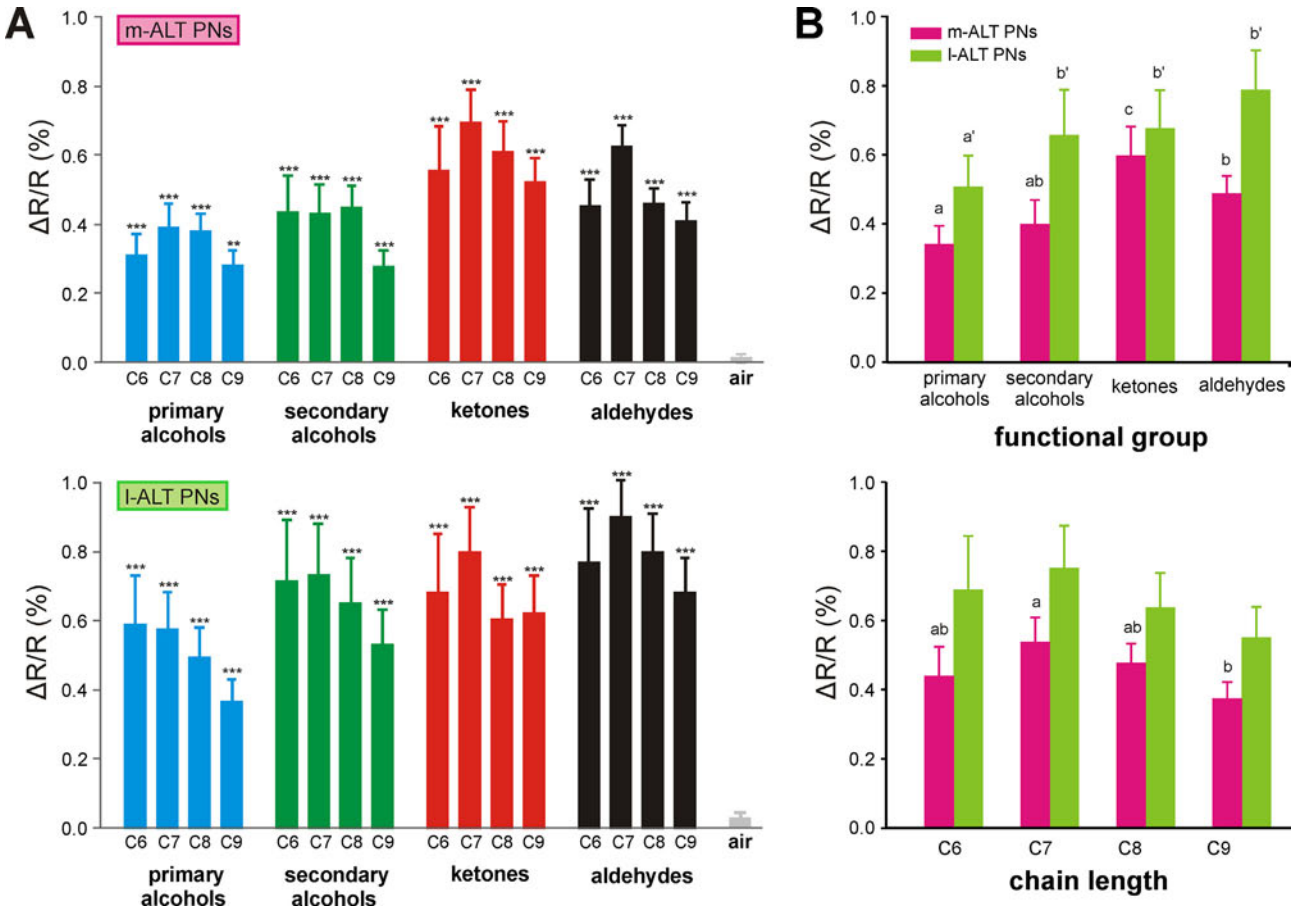

Fig. 2. Odor quality coding – Response intensity. (A) Response amplitude ($\Delta R/R\%$) induced by the 16 aliphatic odorants in m-ALT PNs (top) and l-ALT PNs (bottom). Error bars indicate SEM across animals ($^{**}p < 0.01$; $^{***}p < 0.001$). (B) Mean response amplitude ($\Delta R/R\%$) induced by aliphatic odors depending on their functional group (top) and carbon chain length (bottom) in m-ALT neurons (pink bars), and l-ALT neurons (green bars). Error bars indicate SEM across animals. (For interpretation of the references to color in this figure legend, the reader is referred to the web version of this article.)

neurons, ketones induced higher activation than other functional groups ($p < 0.05$, post hoc Tukey tests), while in l-ALT neurons primary alcohols induced weaker activation than other functional groups ($p < 0.05$, post hoc Tukey tests) (Fig. 2B, upper panel). As a result, the two PN types responded differently to the functional groups of odorants (ANOVA, *functional group* × *PN type* interaction: $F_{3,51} = 5.2$, $p < 0.01$). In the case of the odorants' carbon chain length, we found that m-ALT neurons responded differently according to this variable (Fig. 2B bottom panel, *chain length* ANOVA, $F_{3,24} = 5.9$, $p < 0.01$). Their responses were stronger to C7 than to C9 molecules, and were intermediate for other chain lengths. By contrast, there was only a non-significant trend for the responses of l-ALT neurons ($F_{3,27} = 2.4$, $p = 0.09$). Accordingly, the two neurons types did not differ in the way they responded to carbon chain lengths (ANOVA, *chain length* × *PN type* interaction: $F_{3,51} = 0.39$, NS). Thus the responses of l-ALT neurons, even if not significant, generally followed the same trend as those of m-ALT neurons.

We previously found that at the input of both subsystems, the intensity of odor-evoked activity is highly correlated with the odorants' vapor pressure (Carcaud et al., 2012). We thus evaluated if this is still the case at the PN level, i.e., at the AL output. We found that increasing vapor pressure led to an increase in response intensity both in l-ALT ($R^2 = 0.68$, $z = 1.16$, $p < 0.001$, Fig. 3) and in m-ALT neurons ($R^2 = 0.44$, $z = 0.79$, $p < 0.01$, Fig. 3), thus showing that the dependence of response intensity on odor vapor pressure is maintained through the different processing phases of the m- and l-subsystems.

Spatial coding of odor quality in PNs. To study the spatial coding of odor quality at the PN level, we measured similarity relationships among all odor pairs ($n = 120$) in both PN types. Pixelwise Euclidian distances (a measure of odor dissimilarity, see methods) were used to perform proximity analyses and determine the principal dimensions explaining variance within each dataset (Fig. 4A). In m-ALT neurons (Fig. 4A left), the first dimension (explaining 43.1% of overall variance) separated odors according to their functional group, while the second dimension (25.1% variance) tended to sort odors depending on their chain length. For l-ALT neurons (Fig. 4A right), the first dimension (36.8% variance) clearly sorted odors based on their

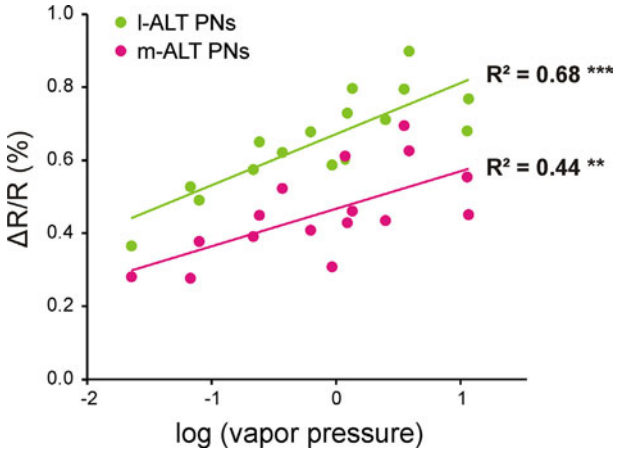

Fig. 3. Responses as a function of odorants' vapor pressure. Correlation between the response amplitude ($\Delta R/R\%$) induced by each of the 16 aliphatic odorants and its vapor pressure. The correlation is significant for both m-APT PNs ($R^2 = 0.44$, $^{**}p < 0.01$) and l-APT PNs ($R^2 = 0.68$, $^{***}p < 0.001$).

carbon-chain length while the second dimension (20.9% variance) clearly separated the different functional groups. Thus, m-ALT and l-ALT neurons relied primarily on different types of information, as shown by the inversion of the first and secondary dimensions across PN types.

We then compared the coding of odorants' chemical features by both PN types by focusing on Euclidian distances between odors with the same or different functional groups (Fig. 4B left). For both PN types, we found lower distances (i.e., higher similarities) for odors with the same functional group than for odors with different functional groups both (Wilcoxon matched pairs test, m-ALT neurons: $z = 2.66$, $p < 0.01$, 8 df; l-ALT neurons: $z = 2.80$, $p < 0.01$, 9 df). This result clearly confirms the capacity of both PN types to encode functional group information. When performing the same kind of analysis for carbon chain length (Fig. 4B right), we found lower distances for odors with the same chain length than for odors with different chain length in l-ALT neurons (Wilcoxon matched pairs test, $z = 2.60$, $p < 0.01$, 9 df), but only a near-significant trend in m-ALT neurons ($z = 1.84$, $p = 0.07$, 8 df). This trend was confirmed by performing a more precise analysis of chain-length coding depending on the difference in the number of carbons between odorants (Fig. 4C). Distances between odor-response maps increased with increasing chain length difference, both for m-ALT neurons (ANOVA $F_{3,24} = 10.8$, $p < 0.001$) and l-ALT neurons (ANOVA $F_{3,27} = 9.7$, $p < 0.001$). Furthermore, the two PN types responded similarly to differences in carbon number (*PN types* × *carbon difference* ANOVA, *PN type* effect: $F_{1,17} = 1.1$, NS, interaction: $F_{3,51} = 2.1$, NS). These results thus suggest that carbon chain length is encoded in both PN types, even though this was clearer in l-ALT neurons (Fig. 4A, C).

Relation between neural and molecular similarity. The above analyses have shown that PN types differ in their encoding of odorant chemical group or chain length, and that each type represents preferentially one of these features (functional group for m-ALT and carbon chain length for l-ALT). Yet, these features are only a small portion of the thousands of potential physico-chemical descriptors of odorant molecules. A previous study calculated *molecular* distances between odorant molecules using 1664 physico-chemical descriptors (Haddad et al., 2008). We next evaluated how well m-ALT and l-ALT PNs represent these molecular distances among odorants. We thus performed a multiple regression analysis with molecular distances (from Haddad et al., 2008) as dependent variable and distances among neural maps in the two PN types and their possible interaction as explanatory variables (Table 1). We found that molecular distances were significantly explained by this model ($R^2 = 0.58$, $p < 0.001$, 116 df). Activity in both l-ALT neurons ($t = 4.38$, $p < 0.001$) and m-ALT neurons ($t = 3.29$, $p < 0.001$) gave a significant outcome, indicating that both PN types are able to represent molecular differences among odorants. However, the interaction between both variables was also significant ($t = -2.14$, $p < 0.05$) suggesting that they contributed differently to the regression with molecular descriptors.

This observation may relate to our finding that the two PN types differentially code odorants' chemical group and carbon chain length. We thus performed the same regression analysis but using (i) only odor pairs which differed in their functional group ($n = 24$ odor pairs) or (ii) only odor pairs which differed in their chain length ($n = 24$ odor pairs). In the first case, the multiple regression analysis showed that only inter-odor similarities measured in m-ALT neurons, and not in l-ALT neurons, accounted for molecular differences in functional group (Table 1, $R^2 = 0.40$; *m-ALT neurons*, $t = 2.68$, $p < 0.05$; *l-ALT neurons*, $t = 1.71$, NS). In the second case, inter-odor similarities measured in l-ALT neurons, and not in m-ALT neurons, accounted for molecular differences in chain length ($R^2 = 0.57$; *l-ALT neurons*, $t = 3.64$, $p < 0.01$; *m-ALT neurons*, $t = 0.32$, NS). Thus, odor distances calculated based on molecular descriptors confirmed the differential processing of molecular features between PN types. The olfactory message conveyed by l-ALT neurons prioritizes information about odorants' carbon chain length, whereas that of m-ALT neurons prioritizes information about odorants' functional group.

Relation between neural and behavioral odor similarity. We next wondered how well activity in both PN pathways relates to honeybees' olfactory behavior. A previous study used appetitive olfactory conditioning to measure generalization responses of bees conditioned to each of the 16 odorants, to any other odorant, allowing the calculation of *behavioral* distances among our 16 odorants (Guerrieri et al., 2005). We thus performed multiple regression analyses with behavioral distances as dependent variable and distances among neural maps in the two PN types and their possible interaction as explanatory variables (Table 1). We found that behavioral distances were significantly explained by this

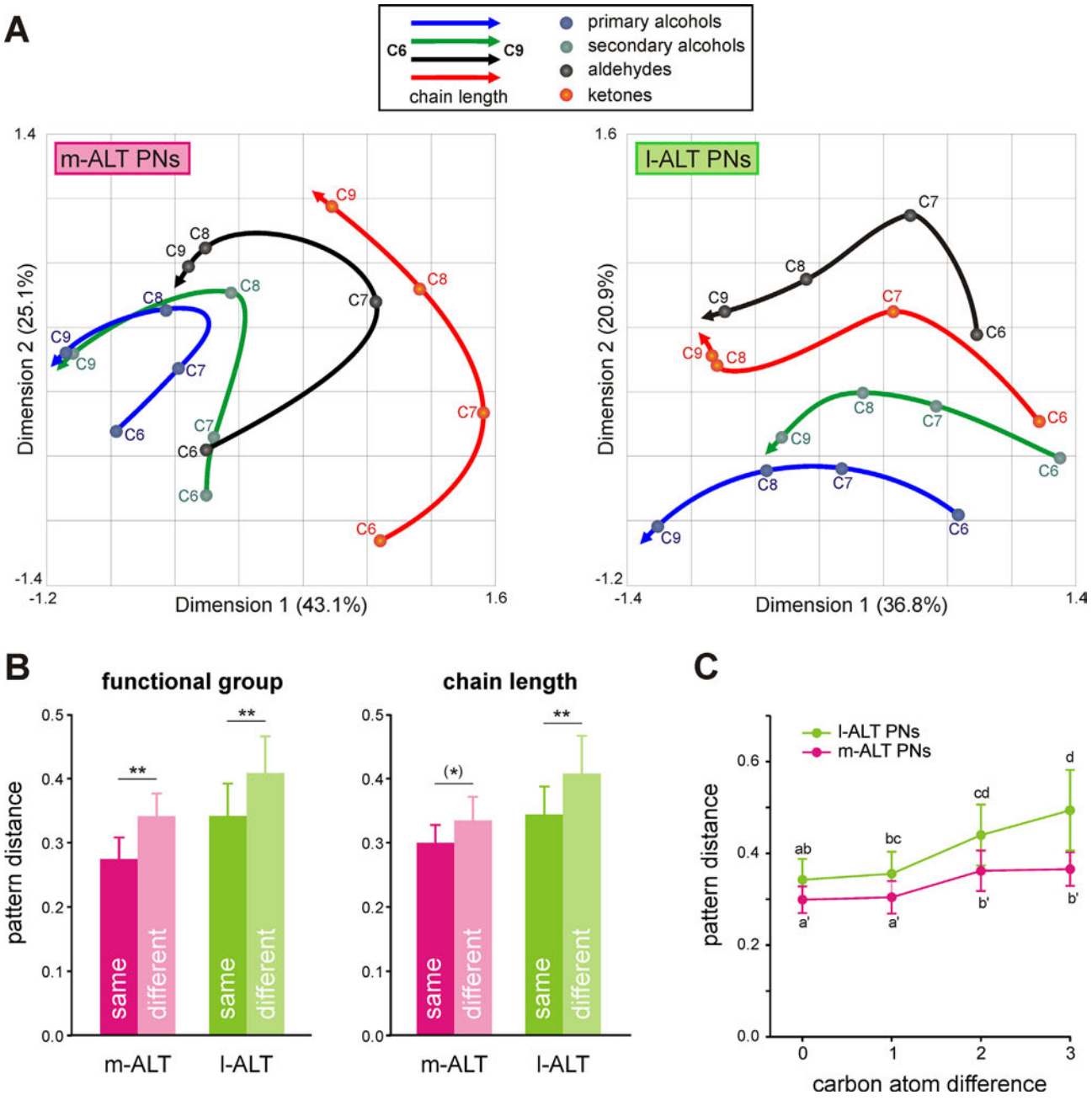

Fig. 4. Odor quality coding – Similarity relationships. (A) Proximity analyses using pixelwise Euclidian distances in m- and l-ALT neurons. Left: For m-ALT neurons, the first dimension (43.1% variance) separates odors depending on their functional group, and the second dimension (25.1% variance) sorts odors depending on their chain length. Right: For l-ALT neurons the first dimension (36.8% variance), separates odors depending on their carbon chain length while the second dimension (20.9% variance) separate odors based on their functional group. (B) Similarity between odors depending on chemical features. Left: Comparison of odors with the same functional group (dark bars) or with different functional groups (light bars), in both m-ALT (pink bars) and l-ALT neurons (green bars). Right: Comparison of odors with the same chain length (dark bars) or with different chain lengths (light bars) ($^{**}p < 0.01$). A near-significant trend is found in m-ALT neurons (*) ($p = 0.06$). (C) Similarity between odors depending on the difference in their carbon numbers, measured for both m-ALT (pink curve) and l- ALT neurons (green curve). (For interpretation of the references to color in this figure legend, the reader is referred to the web version of this article.)

model ($R^2 = 0.53$, $p < 0.001$, 116 df). Activity in l-ALT neurons ($t = 4.37$, $p < 0.001$), m-ALT neurons ($t = 2.69$, $p < 0.01$), as well as their interaction ($t = -2.00$, $p < 0.05$) were all significant. Thus, both PN types can predict bees' olfactory behavior, but each one provides different information for shaping behavioral responses.

Again, this result may relate to our above finding that the two PN types differentially code odorants' chemical group and carbon chain length. We thus asked how well neural odor similarities measured in both PN types predict honeybees' behavior when only one chemical feature differed, either functional group or chain length.

Table 1. Results of multiple regression analyses with molecular distances (after Haddad et al., 2008) or behavioral distances (after Guerrieri et al., 2005) as dependent variable, and distances among neural activity maps in l-ALT PNs, m-ALT PNs and their interaction as explanatory variables. Individual significance of the variables is indicated after t tests. β coefficients are the partial regression coefficients for each variable. $^{*}p < 0.05$; $^{**}p < 0.01$; $^{***}p < 0.001$; NS: non-significant

		l-ALT			m-ALT			l-ALT * m-ALT			R^2	R^2 adjusted	df
		t	Significance	β coefficient	*t*	Significance	β coefficient	*t*	Significance	β coefficient			
Molecular distances Haddad et al. (2008)	All data	4.38	***	0.95	3.29	**	0.85	−2.14	*	−0.87	0.58	0.57	116
	Functional group	1.71	*NS*	0.30	2.68	*	0.47				0.40	0.34	21
	Chain length	3.64	**	0.71	0.32	*NS*	0.06				0.57	0.53	21
Behavioral distances Guerrieri et al. (2005)	All data	4.37	***	1.004	2.69	**	0.73	−2.004	*	−0.86	0.53	0.52	116
	Functional group	1.45	*NS*	0.28	2.10	*	0.40				0.30	0.24	21
	Chain length	2.31	*	0.48	1.39	*NS*	0.29				0.51	0.46	21

When differences in functional group were considered, only distances measured in m-ALT neurons participated significantly in the regression (Table 1, $R^2 = 0.30$; *m-ALT neurons*, $t = 2.10$, $p < 0.05$; *l-ALT neurons,* $t = 1.45$, NS). When differences in chain length were considered, only distances measured in l-ALT neurons participated significantly ($R^2 = 0.51$; *l-ALT neurons*, $t = 2.31$, $p < 0.05$; *m-ALT neurons*, $t = 1.39$, NS). These results confirm our above analyses at the molecular level, and show that both PN types differ in their contribution to olfactory behavior: while m-ALT neurons provide information about the functional group of odorants, l-ALT neurons inform about their carbon chain length.

AL transformation of odor quality coding. We then asked how AL networks affect odor coding and thus focused on a comparison between input and output for both the m- and the l-subsystem. We first found that the intensities of odor-evoked signals were mostly conserved between input and output, with the same level of correlation in the m-subsystem (Fig. 5A left, $R^2 = 0.54$, $z = 0.93$, $p < 0.01$) and the l-subsystem (Fig. 5A right, $R^2 = 0.53$, $z = 0.92$, $p < 0.01$). We then evaluated how AL networks affected the qualitative nature of odor representation. We thus correlated the Euclidian distances measured at the PN level (AL output) with those emphasizing ORN responses (AL input), which we measured in a previous work (Carcaud et al., 2012). Similarity relationships among odorants were correlated between AL input and output, both in the m-subsystem (Fig. 5B left, $R^2 = 0.35$, Mantel test, $p < 0.001$) and in the l-subsystem (Fig. 5B right, $R^2 = 0.61$, Mantel test, $p < 0.001$), showing that transformation by AL networks generally conserves similarity relationships. However, the correlation observed for the m-subsystem was significantly weaker than for the l-subsystem (homogeneity test, $p < 0.01$), thus showing a stronger reshaping of odor-similarity relationships in the network associated with m-ALT neurons.

To explore qualitative changes in both subsystems, we performed cluster analyses on odor-similarity relationships. For m-ALT neurons, the analysis confirmed a clear segregation based on functional group (Fig. 5C left, "output"). A comparison with the cluster analysis performed on data emphasizing ORN responses (Fig. 5C left, "input"; from (Carcaud et al., 2012)) shows that the difference induced by local processing was a redistribution of aldehydes among other odors and the appearance of a secondary segregation based on chain length. For l-ALT neurons (Fig. 5C right, "output"), the cluster analysis provided very similar results as the one performed on data dominated by ORN responses (Fig. 5C right, "input"), thus indicating less reshaping by local processing. In both cases, we observed a clear separation depending on chain length (C6–C7 vs. C8–C9), but with a separate clustering of aldehydes. These analyses confirmed the previous result showing a stronger AL processing in the m-subsystem.

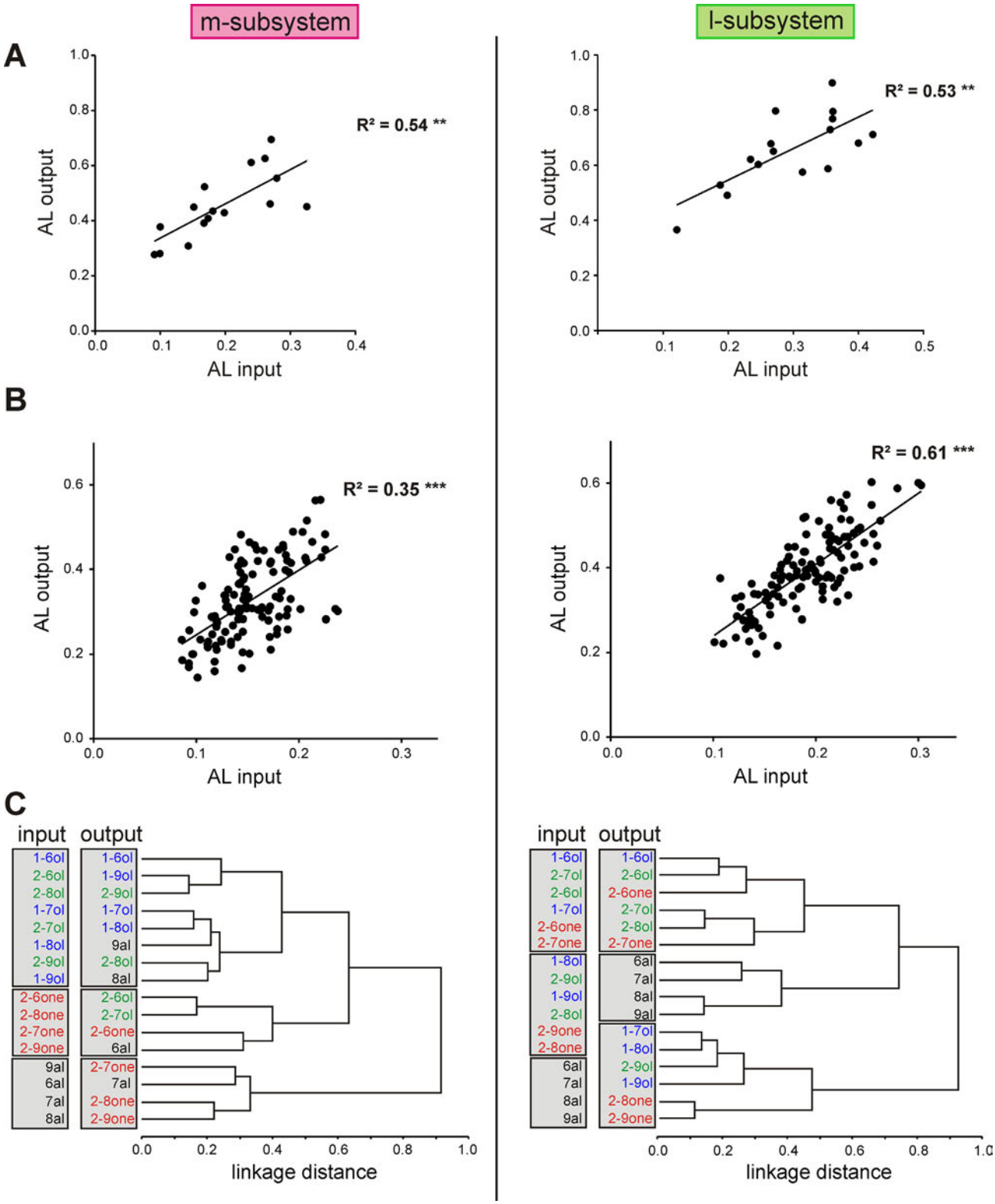

Fig. 5. Odor quality coding – Comparison of input and output similarity relationships. (A) Correlation between the amplitudes of odor-induced responses to the 16 aliphatic odorants at AL input ($\Delta F/F$ %, Carcaud et al., 2012) and output (ΔR/R%, PN recordings, this study) for the m-subsystem (left, $R^2 = 0.54$, $^{**}p < 0.001$) and for the l-subsystem (right, $R^2 = 0.53$, $^{**}p < 0.001$). (B) Correlation of Euclidian distances between odors obtained at AL input (Carcaud et al., 2012) and output (this study) for the m-subsystem (left, $R^2 = 0.35$, $^{***}p < 0.001$) and for the l-subsystem (right, $R^2 = 0.61$, $^{**}p < 0.001$). (C) Cluster analysis based on pixelwise Euclidian distances among odor response maps (using Ward's classification method) showing similarity relationships among odors at the input and at the output of the AL, in both m-subsystem (left, input: $N = 8$; output: $N = 9$) and l-subsystem (right, input: $N = 7$; output: $N = 10$). In both analyses, functional groups are color-coded: primary alcohols in blue, secondary alcohols in green, aldehydes in black and ketones in red. (For interpretation of the references to color in this figure legend, the reader is referred to the web version of this article.)

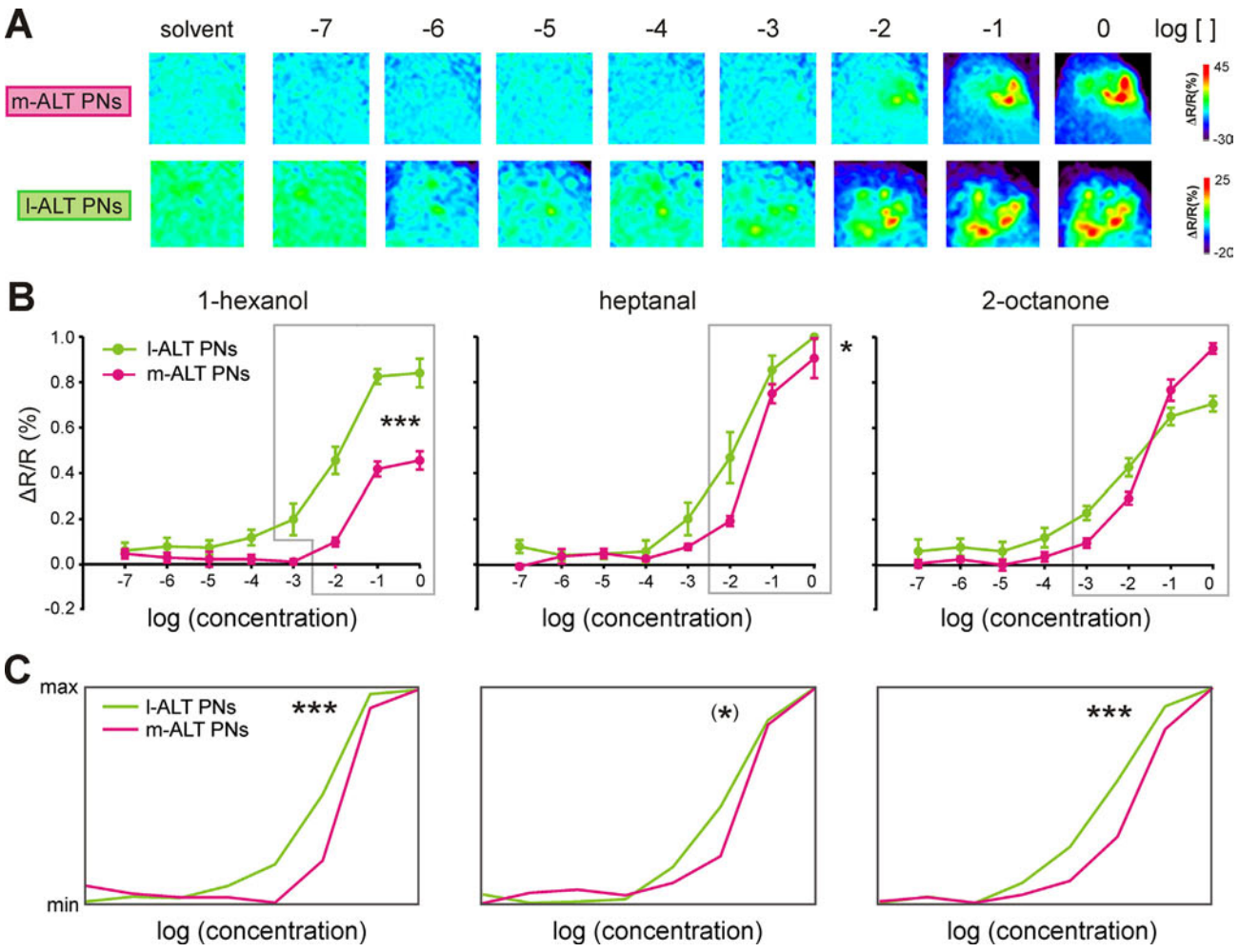

Fig. 6. Odor quantity coding – Response intensity as a function of concentration. (A) Activity maps of odor-induced calcium signals to solvent and to increasing concentrations of 2-octanone measured in m-ALT PNs (top) and l-ALT PNs (bottom). Relative fluorescence changes ($\Delta R/R\%$) are presented in a false-color code, from dark blue to red. (B) Dose–response curves to the three odorants at eight concentrations are shown after normalization to the strongest odor response within each animal. Relative fluorescence changes ($\Delta R/R\%$) depending on concentration for 1-hexanol (left), heptanal (middle) and 2-octanone (right). In the three doses–response curves, concentrations of each odorant which induce a significantly higher signal than the air control are surrounded by a gray line ($^{***}p < 0.001$). (C) Curves in (B) normalized to the same minimum and maximum ($^{***}p < 0.001$). (For interpretation of the references to color in this figure legend, the reader is referred to the web version of this article.)

Transformation of odor quantity information

In a second experiment, we returned to the PN level and explored odor quantity coding in m-ALT and l-ALT PNs by stimulating bees with 3 odorants (1-hexanol, heptanal and 2-octanone) at 8 concentrations (10^{-7} to 10^{0} dilutions). As shown in Fig. 6A, increasing odorant concentration (here for 2-octanone) led to an increase in the number of activated glomeruli in both m-ALT and l-ALT PNs, and thus to an increase of global AL activity (Fig. 6B). The same increase was observed for the two other odorants, 1-hexanol and heptanal, in both m-ALT and l-ALT neurons (Fig. 6B).

Dose–response curves in PNs. To facilitate the comparison of the dose–response curves obtained for m-ALT and l-ALT neurons, global response amplitudes were normalized to the maximum response to any odorant within each honeybee (Fig. 6C). For the three tested odorants, a significant increase in response intensity with increasing odor concentrations was found in both m-ALT neurons (ANOVA, $F_{8,40} > 55.6$, $p < 0.001$) and l-ALT neurons ($F_{8,40} > 65.9$, $p < 0.001$). The first concentrations which induced responses that were significantly higher than those elicited by the control (mineral oil) were 10^{-2} and 10^{-3} for 1-hexanol in m- and l-ALT neurons respectively, 10^{-2} for heptanal and 10^{-3} for 2-octanone in both PN types (post hoc Dunnett tests, $p < 0.05$). However, depending on the odorant, m- or l-ALT neurons showed different dose–response curves (Fig. 6B). While l-ALT neurons displayed significantly higher activity than m-ALT neurons in response to 1-hexanol and heptanal (*PN type* × *concentration* ANOVA, *PN type* effect, $F_{1,9} = 33.01$, $p < 0.001$ and $F_{1,9} = 7.38$, $p < 0.05$ respectively), no difference appeared for 2-octanone ($F_{1,9} = 0.46$, NS). These results agree with those of the first experiment, in which 1-hexanol and heptanal elicited comparatively more activity in l-ALT than in m-ALT PNs (see Fig. 2A). We found, however, that

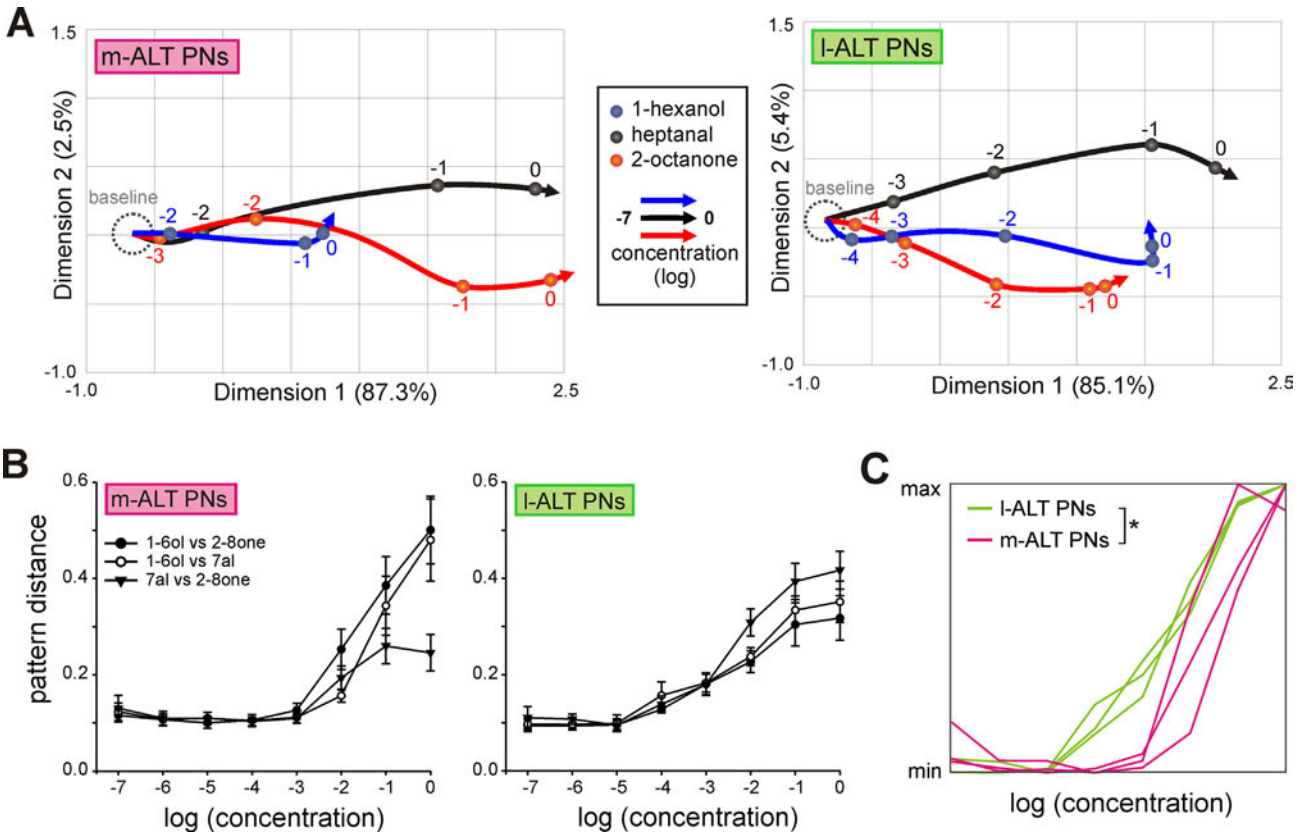

Fig. 7. Odor quantity coding – similarity relationships. (A) Proximity analysis using the 276 Euclidian distances arising from the three odors at eight concentrations. For both m-ALT neurons (left) and l-ALT neurons (right), a first dimension separates odors depending on their concentration (arrows pointing to the right, 87.3% and 85.1% variance respectively). (B) Distances between odor-evoked patterns at each concentration (1-hexanol vs heptanal, 1-hexanol vs 2-octanone and heptanal vs 2-octanone), depending on the concentration (log), in m-ALT PNs (left) and l-ALT PNs (right). (C) Curves in (B) normalized to the same minimum and maximum ($^{*}p < 0.05$).

responses of m- and l-ALT PNs developed differently as a function of concentration, for 1-hexanol and 2-octanone (Fig. 6C, *PN type* × *concentration* interaction, $F_{7,63} = 15.04$, $p < 0.001$ and $F_{7,63} = 11.8$, $p < 0.001$, respectively). This trend only reached near-significance for heptanal ($F_{7,63} = 2.07$, $p = 0.06$). In all cases, l-ALT neurons showed more gradual dose–response curves than m-ALT neurons (Fig. 6C).

Similarity relationships as a function of concentration. We next studied similarity relationships among all stimulus pairs ($n = 276$) in both PN types using pixelwise Euclidian distances. We first performed proximity analyses and determined the main dimensions explaining most of the variance within each dataset (Fig. 7A). The two main dimensions explained 89.8% and 90.5% of overall variance in m- and l-ALT neurons, respectively. In m-ALT neurons (Fig. 7A, left) as well as in l-ALT neurons (Fig. 7A, right), the first dimension (87.3% and 85.1% variance, respectively) was clearly related to odorant concentration. The second dimension segregated the three odorants based on their chemical identity, both in m-ALT neurons (2.5% variance) and l-ALT neurons (5.4% variance). Increasing concentrations are represented in the figure with arrows of a different color for each odorant. L-ALT neurons displayed a gradual distribution of odor representations along an increasing concentration gradient, clearly segregating representations from 10^{-4} to 10^{0}. By contrast, m-ALT neurons showed only a steep transition from 10^{-2} to 10^{-1} and 10^{0}. Thus, the differences in concentration–response relationships observed above between PN types directly affected similarity relationships among odor concentration maps.

We then studied the evolution of similarity relationships with increasing concentration using Euclidian distances between the three pairs of odorants (1-hexanol vs. heptanal, 1-hexanol vs. 2-octanone, and heptanal vs. 2-octanone) when the two members of a pair had the same concentration (Fig. 7B). As expected, distances between odorants increased, i.e., odor patterns became less similar, with increasing concentration both in m-ALT neurons (Fig. 7B, *odor pair* × *concentration* ANOVA, *concentration* effect, $F_{7,35} = 28.4$, $p < 0.001$) and in l-ALT neurons ($F_{7,28} = 36.3$, $p < 0.001$). However, distances did not evolve at the same pace as a function of concentration in m- and l-ALT PNs (ANOVA *odor pair* × *concentration* × *PN type*, *concentration* × *PN type* interaction, $F_{7,63} = 2.2$, $p < 0.05$). Again, distances increased more gradually and provided a finer description of odor concentration in l-ALT neurons than in m-ALT neurons (Fig. 7B, C).

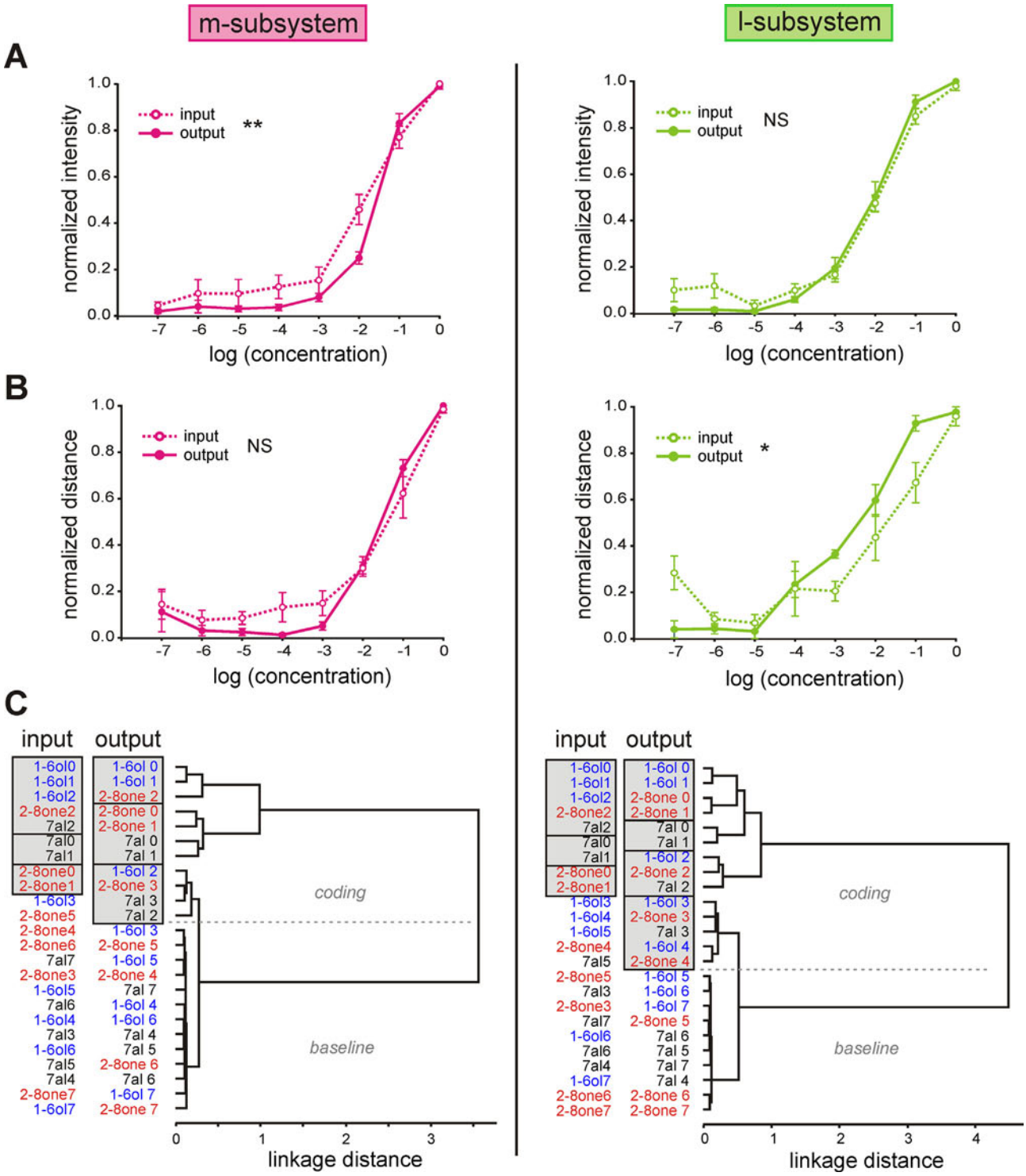

Fig. 8. Odor quantity coding – Comparison of input and output intensity and similarity relationships. (A) Comparison of response intensity as a function of odorant concentration at the input and output in the m-subsystem (left) and in the l-subsystem (right) ($^{**}p < 0.01$). (B) Comparison of inter-odor distance as a function of odorant concentration at the input and output in the m-subsystem (left) and in the l-subsystem (right) ($^{*}p < 0.05$). (C) Cluster analysis based on pixelwise Euclidian distances among odor response maps (using Ward's classification method) showing similarity relationships among odors at different concentrations in both PN types. Left: m-subsystem (input: $N = 8$; output: $N = 6$). Right: l-subsystem (input: $N = 7$; output: $N = 5$).

AL transformation of odor quantity coding. Finally, we asked if and how information on odorant concentration was reshaped by local AL networks associated with m- and l-ALT neurons, i.e., from the receptor to the PN level. To this end, we compared dose–response curves analyzed above (AL output) with those obtained for responses dominated by ORNs (AL input, Carcaud et al., 2012). We first addressed the transformation of

response intensity in both subsystems (Fig. 8A). We averaged the dose–response curves of the three odorants within each animal. Then we normalized each resulting curve so that its minimum was 0 and its maximum 1. We found clear evidence for a significant transformation of the dose–response relationship in the m-ALT subsystem (*AL level* × *concentration* ANOVA, interaction, $F_{7,84} = 2.90$, $p < 0.01$), but not in the l-ALT subsystem (interaction, $F_{7,77} = 1.30$, NS). A regression analysis which allowed calculating Hill coefficients confirmed a significant difference between input and output for the former (Fig. 8A left, 0.65 ± 0.11 and 1.74 ± 0.63 respectively, Mann–Whitney test, $z = 2.58$, $p < 0.01$) but not for the latter (Fig. 8A right, 0.73 ± 0.09 and 0.89 ± 0.20 respectively, Mann-Whitney test, $z = 0.25$, NS). Thus, local processing within the m-subsystem produced steeper dose–response relationships at the output of the AL (e.g., higher Hill coefficients; Fig. 8A, left), while processing in the l-subsystem did not modify intensity responses (Fig. 8A, right).

We then asked how these changes in dose–response relationships in the two subsystems translate into odorant differentiation at each concentration (Fig. 8B). We thus averaged and normalized Euclidian distances as above (Fig. 8A) and compared input and output signals. We found a similar evolution of inter-odor distances as a function of odorant concentration at the input and output of the m-subsystem (Fig. 8B left; *AL level* × *concentration* ANOVA, interaction, $F_{7,84} = 0.97$, NS). On the contrary, for the l-subsystem we found a significant transformation of inter-odor distances as depending on odorant concentration between AL input and output (Fig. 8B right; interaction, $F_{7,77} = 2.68$, $p < 0.05$). Again, these analyses were confirmed by the comparisons of Hill coefficients, which showed a significant difference between input and output for the l-subsystem (1.43 ± 0.44 and 0.46 ± 0.07 respectively, Mann-Whitney test, $z = 2.37$, $p < 0.05$) but not for the m-subsystem (1.08 ± 0.52 and 0.87 ± 0.12 respectively, Mann–Whitney test, $z = 0.91$, NS). We conclude that reshaping of odorant information within the l-subsystem provides a more graded variation of inter-odor distances with odor concentration (e.g., lower Hill coefficients) at the AL output than at its input.

To further explore the transformation of qualitative coding of odorants at different concentrations, we performed cluster analyses on Euclidian distances (Ward's method; Fig. 8C). For both PN types, the analyses first separated odors depending on their concentration, with high concentrations ($\geq 10^{-2}$) in one cluster and low concentrations in the other (the latter are called baseline as they do not induce significant activity in comparison to the solvent, between 10^{-4} and 10^{-7}). In both PN types, a small subcluster grouped intermediate concentrations (10^{-4} and 10^{-3} for m-ALT neurons, 10^{-3} and 10^{-2} for l-ALT neurons). In m-ALT neurons (Fig. 8C left), as well as in l-ALT neurons (Fig. 8C right), the odors also clustered depending on their chemical identity, each odorant at the highest concentrations being placed in a different subgroup. When these cluster analyses were compared with those performed on the input data (Fig. 8C, "input"), the same organization was observed for high concentrations, but a specific cluster for intermediate concentrations was absent at the input. These results show that significant processing takes place within subsystems, providing a finer coding of odor concentration in m-ALT PNs, and contrast enhancement relative to baseline in l-ALT PNs.

DISCUSSION

We recorded neural activity of m-ALT and l-ALT projections neurons (PNs) to a standard panel of aliphatic odorants differing in two chemical features (functional group and carbon chain length) or in their concentration. Our results show differential coding rules and a different transformation of odor information in the two subsystems, supporting the existence of parallel processing (see Introduction) by the two pathways.

Odor quality coding

While our previous recordings at the AL input revealed a tendency for segregation between the two pathways in the coding of odorants' functional group and chain length (Carcaud et al., 2012), our data at the PN level, i.e., at the AL output, show a more contrasted picture, suggesting that processing by AL networks strengthened this dichotomy. Functional group information is clearly dominant in the responses of m-ALT PNs, while chain length information is dominant in those of l-ALT PNs. Even though the other feature is also represented within each pathway, the two subsystems provide higher order brain centers with different, but complementary portions of odor quality information.

The first strong support for this idea comes from the regression analysis performed with chemical distances among odorant molecules (Haddad et al., 2008). These physicochemical measures can only be represented correctly by taking into account data from both subsystems at the same time (Table 1). In addition, when odor pairs were sorted according to their chemical features, chemical distances between odorants that differed in their functional group were only significantly predicted by neural distances in m-ALT PNs, while chemical distances of odorants that differed in their chain length were only significantly predicted by neural distances in l-ALT PNs. Thus, even though neural distances can be different for different functional groups in l-ALT PNs (Fig. 4B), these differences are not good descriptors of the *chemical* differences existing among these molecules. Each subsystem provides, therefore, a faithful molecular description of chain-length and of functional group to higher brain centers.

The second support comes from the regression analysis performed with the generalization behavior of honeybees in an appetitive conditioning experiment (Guerrieri et al., 2005). Behavioral distances among odorants that differed in their functional group were only significantly predicted by neural distances in m-ALT PNs, while chemical distances among odorants that differed in their chain length were only significantly predicted by distances

in l-ALT PNs. Most importantly, both subsystems significantly contributed to the regression. Thus, we conclude that both subsystems are necessary for the bees to respond finely to differences in both chain length and functional group. In our regression analyses, the interaction between l-ALT and m-ALT was significant, suggesting that both PN types do not contribute in a linear manner to explain behavioral distances. This observation indicates rather complex additional processing within higher order centers (the mushroom bodies, for instance), which would bind again information from both pathways for shaping the bees' behavioral responses. This parallel processing would apply for the many odorants that are detected and processed by both subsystems. There are, however, a few odorants, mostly pheromones, that seem to only be processed by one subsystem: queen pheromone components by l-ALT PNs and brood pheromone components mainly by m-ALT PNs (Carcaud et al., 2015). It may be that some odorants with a strong biological value for bees do not undergo parallel processing like the general odorants we tested. As brood pheromone is composed of long-chain esters and queen pheromone of decenoic acids and aromatic molecules, one may wonder if this difference relates to their pheromonal nature or rather to their specific chemical quality. Future work including pheromonal and non-pheromonal compounds with a similar chemical structure may help clarifying this point.

Odor quantity coding

Our results confirm the clear concentration dependency of l-ALT PNs previously found, when only these PNs were accessible to calcium imaging (Sachse and Galizia, 2003). Most importantly, they reveal a different behavior of m-ALT PNs with respect to concentration changes, with a steeper transition from baseline to maximal response in these neurons (Fig. 6B, C). Concerning similarity relationships among odorants, we found that Euclidian distances increased with increasing concentrations in both PN types (Fig. 7B). This is due to the recruitment of new glomeruli with increasing odor concentration, as commonly observed in insects (Sachse and Galizia, 2003; Wang et al., 2003) and vertebrates (Friedrich and Korsching, 1997; Rubin and Katz, 1999). This has the effect of enhancing the separability of odor representations, improving odor discrimination (Strauch et al., 2012). We observed, however, that inter-odor distances increased more smoothly in l-ALT than in m-ALT PNs (Fig. 7C), fitting with the observation that the intensity of glomerular responses increased more gradually in the former than in the latter PN type (Fig. 6C). Such clear distinction between the concentration dependencies of the two subsystems was absent at AL input (Carcaud et al., 2012). Our comparisons of dose–response curves between ORN and PN levels show that AL processing induces a steeper transition (higher Hill coefficient) in the m-subsystem, but did not affect the l-subsystem (Fig. 8A), and that it improved inter-odor similarity relationships at higher concentrations in the l-subsystem (Fig. 8B). This observation provides experimental support to the hypothesis that processing of odor information by local networks may be different in the two AL subsystems (Galizia and Rössler, 2010; Schmuker et al., 2011).

Local processing in the AL: segregated vs shared inhibition

In the honey bee, AL processing is performed by ~4000 local interneurons (LNs) (Witthöft, 1967), which respond faster than PNs and are thus able to reshape the olfactory message transmitted by PNs to higher order centers (Krofczik et al., 2009; Girardin et al., 2013). Many LNs are GABAergic (~800) with a fairly uniform distribution across glomeruli (Schafer and Bicker, 1986). A small set of LNs (~35) is histaminergic, and similarly innervates many AL glomeruli (Bornhauser and Meyer, 1997), creating a second inhibitory circuit (Sachse et al., 2006). The remaining LNs have one or several as yet unidentified neurotransmitters, which may include glutamate and a range of neuropeptides (Galizia and Kreissl, 2012). Two morphological types of LNs were described (Fonta et al., 1993; Sachse and Galizia, 2002): *Homogeneous LNs* innervating diffusely many (30–100) glomeruli, and *heterogeneous LNs* innervating densely one glomerulus and other glomeruli only sparsely. Based on this dissociation, two separate inhibitory networks with different effects on odor representation were hypothesized: (1) a GABAergic network, probably supported by homogeneous LNs, would carry out a global gain control, modifying the intensity of the response over the whole AL, without modifying the relative activity of glomeruli; (2) a second network, supported by heterogeneous LNs, would contrast-enhance glomerular responses at the output of the AL through lateral inhibition and modify relative glomerular responses in the pattern (Sachse and Galizia, 2002). Using a computational network model, a previous study proposed that the differences in physiological properties found between l-ALT and m-ALT boutons in the mushroom body calyx (Yamagata et al., 2009) could be attributed to different AL network effects (Schmuker et al., 2011). This model proposed that strong lateral inhibition would provide good odor discrimination to l-ALT PNs boutons, whereas weak lateral inhibition would only support weak odor discrimination in m-ALT PNs. Contrarily, we found evidence for a stronger transformation of inter-odor distances in the m-subsystem compared to the l-subsystem (Fig. 5B). In our view, such a transformation has to be the result of strong lateral inhibition, which goes against the hypothesis of only a weak lateral inhibition in the m-subsystem (Schmuker et al., 2011). We rather favor the idea that substantial local processing indeed takes place in both AL subsystems, although it may still follow different rules within each subsystem.

While most LNs are known to innervate both AL halves, a few individually-reconstructed LNs were shown to be restricted to only one subsystem (Meyer, 2011). Such neurons could be the basis for specific processing within one subsystem. The fact that most LNs cross the two halves of the AL, however suggests that the two subsystems exchange a substantial amount of information. We observed a possible product of this cross-influence between subsystems, with a better coding of chain length information in m-ALT PNs (Fig. 6B, C)

than what was observed at the input (Carcaud et al., 2012). One could imagine that local processing only sharpened already existing, subtle, differences between the maps of odors within different chain lengths in this subsystem. However, another probable explanation is that LNs that were activated by glomeruli of the l-subsystem provided inhibitory, chain-length containing, information to glomeruli of the m-subsystem. Thus, chain length-dependent cross-inhibition could convey improved chain-length coding to the m-subsystem. These observations suggest that possible differences in processing between l- and m-subsystems should be understood as a product of local specificities in inhibitory networks, but also in possibly asymmetric influences of one subsystem on the other. A better knowledge of the different types of LNs (Meyer, 2011) as well as of their neurotransmitters (Schafer and Bicker, 1986; Bornhauser and Meyer, 1997), may allow performing dedicated pharmacological experiments linked to optical imaging (Girardin et al., 2013) in both subsystems to disentangle the multiple influences that each PN type receives through AL processing.

CONCLUSION

This study addressed the influence of AL networks on the spatial coding of odor quality and odor quantity in the dual olfactory system of the honey bee brain, using *in vivo* calcium imaging. We have shown that m-ALT and l-ALT PNs are in part specialized to provide information about different chemical features influencing the coding of odor quality: functional group and chain length. To definitely demonstrate the differential role of these pathways in shaping bees' olfactory behavior, a lesioning strategy is needed. Theoretically, we would expect a lower accuracy of bees' behavioral responses as a function of chain-length or functional group when lesioning the l-ALT the m-ALT respectively. We started applying such a strategy using manual lesions on the m-ALT tract in a recent study (Carcaud et al., 2016). The results showed that m-ALT lesion strongly impairs bees' ability to learn an odor-sucrose association, suggesting that in addition to the qualitative coding of odor information demonstrated here, the m-ALT (and possibly also the l-ALT) may be crucial for intact odor learning. Further efforts should be invested in this direction, attempting to improve the size and precision of the lesions, possibly using 2-photon laser-mediated microdissection.

ACKNOWLEDGMENTS

we thank Maud Combe for developing the custom programs used for data analysis. We also thank the ANR (Projects EVOLBEE, 2010-BLAN-1712-01 and Bee-o-CHOC, 17-CE20-0003 to J.C.S; Project MINICOG, 13-BSV4-0004 to M.G.), the French Research Ministry (J.C.), the French National Research Council (CNRS), University Paul Sabatier and the Institut Universitaire de France (M.G.) for support.

REFERENCES

Abel R, Rybak J, Menzel R (2001) Structure and response patterns of olfactory interneurons in the honeybee, *Apis mellifera*. J Comp Neurol 437:363–383.

Ache BW, Young JM (2005) Olfaction: diverse species, conserved principles. Neuron 48:417–430.

Adam Y, Livneh Y, Miyamichi K, Groysman M, Luo L, Mizrahi A (2014) Functional transformations of odor inputs in the mouse olfactory bulb. Front Neural Circ 8:129.

Bhandawat V, Olsen SR, Gouwens NW, Schlief ML, Wilson RI (2007) Sensory processing in the Drosophila antennal lobe increases reliability and separability of ensemble odor representations. Nat Neurosci 10:1474–1482.

Bornhauser BC, Meyer EP (1997) Histamine-like immunoreactivity in the visual system and brain of an orthopteran and a hymenopteran insect. Cell Tissue Res 287:211–221.

Brill MF, Rosenbaum T, Reus I, Kleineidam CJ, Nawrot MP, Rossler W (2013) Parallel processing via a dual olfactory pathway in the honeybee. J Neurosci 33:2443–2456.

Brill MF, Meyer A, Rossler W (2015) It takes two-coincidence coding within the dual olfactory pathway of the honeybee. Front Physiol 6:208.

Carcaud J, Hill T, Giurfa M, Sandoz JC (2012) Differential coding by two olfactory subsystems in the honey bee brain. J Neurophysiol 108:1106–1121.

Carcaud J, Giurfa M, Sandoz JC (2015) Differential combinatorial coding of pheromones in two olfactory subsystems of the honey bee brain. J Neurosci 35:4157–4167.

Carcaud J, Giurfa M, Sandoz JC (2016) Parallel olfactory processing in the honey bee brain: odor learning and generalization under selective lesion of a projection neuron tract. Front Integr Neurosci 9(75):1–13.

Deisig N, Giurfa M, Sandoz JC (2010) Antennal lobe processing increases separability of odor mixture representations in the honeybee. J Neurophysiol 103:2185–2194.

Fonta C, Sun XJ, Masson C (1993) Morphology and spatial distribution of bee antennal lobe interneurones responsive to odours. Chem Senses 18(2):101–119.

Friedrich RW, Korsching SI (1997) Combinatorial and chemotopic odorant coding in the zebrafish olfactory bulb visualized by optical imaging. Neuron 18:737–752.

Galizia CG, Kreissl S (2012) Neuropeptides in honey bees. In: Honeybee neurobiology and behavior. Springer. p. 211–226.

Galizia CG, Rössler W (2010) Parallel olfactory systems in insects: anatomy and function. Annu Rev Entomol 55:399–420.

Galizia CG, Vetter RS (2004) Optical methods for analyzing odor-evoked activity in the insect brain. In: Christensen TA, editor. Methods in insect sensory neuroscience. Boca Raton: CRC Press. p. 345–392.

Gao Q, Yuan B, Chess A (2000) Convergent projections of drosophila olfactory neurons to specific glomeruli in the antennal lobe. Nature Neurosci 3:780–785.

Girardin CC, Kreissl S, Galizia CG (2013) Inhibitory connections in the honeybee antennal lobe are spatially patchy. J Neurophysiol 109:332–343.

Grabe V, Baschwitz A, Dweck HK, Lavista-Llanos S, Hansson BS, Sachse S (2016) Elucidating the neuronal architecture of olfactory glomeruli in the *Drosophila* antennal lobe. Cell Rep 16:3401–3413.

Guerrieri F, Schubert M, Sandoz JC, Giurfa M (2005) Perceptual and neural olfactory similarity in honeybees. PLOS Biol 3:e60.

Haberly LB, Price JL (1977) The axonal projection patterns of the mitral and tufted cells of the olfactory bulb in the rat. Brain Res 129:152–157.

Haddad R, Khan R, Takahashi YK, Mori K, Harel D, Sobel N (2008) A metric for odorant comparison. Nat Methods 5:425–429.

Hansson BS, Anton S (2000) Function and morphology of the antennal lobe: new developments. Ann Rev Entomol 45:203–231.

Hildebrand JG, Shepherd GM (1997) Mechanisms of olfactory discrimination: converging evidence for common principles across phyla. Ann Rev Neurosci 20:595–631.
Igarashi KM, Ieki N, An M, Yamaguchi Y, Nagayama S, Kobayakawa K, Kobayakawa R, Tanifuji M, Sakano H, Chen WR, Mori K (2012) Parallel mitral and tufted cell pathways route distinct odor information to different targets in the olfactory cortex. J Neurosci 32:7970–7985.
Imai T, Sakano H (2007) Roles of odorant receptors in projecting axons in the mouse olfactory system. Curr Opin Neurobiol 17:507–515.
Joerges J, Küttner A, Galizia CG, Menzel R (1997) Representations of odours and odour mixtures visualized in the honeybee brain. Nature 387:285–288.
Kanzaki R, Arbas EA, Strausfeld NJ, Hildebrand JG (1989) Physiology and morphology of projection neurons in the antennal lobe of the male moth *Manduca sexta*. J Comp Physiol A 165:427–453.
Kim AJ, Lazar AA, Slutskiy YB (2015) Projection neurons in *Drosophila* antennal lobes signal the acceleration of odor concentrations. eLife 4 06651.
Kirschner S, Kleineidam CJ, Zube C, Rybak J, Grunewald B, Rössler W (2006) Dual olfactory pathway in the honeybee, *Apis mellifera*. J Comp Neurol 499:933–952.
Krofczik S, Menzel R, Nawrot MP (2009) Rapid odor processing in the honeybee antennal lobe network. Front Comput Neurosci 2:9.
Laurent G (2002) Olfactory network dynamics and the coding of multidimensional signals. Nat Rev Neurosci 3:884–895.
Meyer A (2011) Characterisation of local interneurons in the antennal lobe of the honeybee PhD Thesis. University of Konstanz.
Mori K, Sakano H (2011) How is the olfactory map formed and interpreted in the mammalian brain? Annu Rev Neurosci 34:467–499.
Mota T, Gronenberg W, Giurfa M, Sandoz JC (2013) Chromatic processing in the anterior optic tubercle of the honey bee brain. J Neurosci 33:4–16.
Müller D, Abel R, Brandt R, Zockler M, Menzel R (2002) Differential parallel processing of olfactory information in the honeybee, *Apis mellifera* L. J Comp Physiol A 188:359–370.
Nagel KI, Wilson RI (2016) Mechanisms underlying population response dynamics in inhibitory interneurons of the *Drosophila* antennal lobe. J Neurosci 36:4325–4338.
Nassi JJ, Callaway EM (2009) Parallel processing strategies of the primate visual system. Nat Rev Neurosci 10(5):360–372.
Pinching AJ, Powell TP (1971) The neuropil of the glomeruli of the olfactory bulb. J Cell Science 9:347–377.
Puopolo M, Belluzzi O (1998) Inhibitory synapses among interneurons in the glomerular layer of rat and frog olfactory bulbs. J Neurophysiol 80:344–349.
Rauschecker JP, Tian B (2000) Mechanisms and streams for processing "what" and "where" in auditory cortex. Proc Natl Acad Sci U S A 97:11800–11806.
Rössler W, Brill MF (2013) Parallel processing in the honeybee olfactory pathway: structure, function, and evolution. J Comp Physiol A 199(11):981–996.
Rubin BD, Katz LC (1999) Optical imaging of odorant representations in the mammalian olfactory bulb. Neuron 23:499–511.
Rybak J (2012) The digital honey bee brain atlas. In: Galizia CG, Eisenhardt D, Giurfa M, editors. Honeybee Neurobiology and Behavior. Netherlands: Springer. p. 125–140.
Sachse S, Galizia CG (2002) The Role of inhibition for temporal and spatial odor representation in olfactory output neurons: a calcium imaging study. J Neurophysiol 87:1106–1117.
Sachse S, Galizia CG (2003) The coding of odour-intensity in the honeybee antennal lobe: local computation optimizes odour representation. Eur J Neurosci 18:2119–2132.
Sachse S, Peele P, Silbering AF, Guhmann M, Galizia CG (2006) Role of histamine as a putative inhibitory transmitter in the honeybee antennal lobe. Front Zool 3:22.
Schafer S, Bicker G (1986) Distribution of GABA-like immunoreactivity in the brain of the honeybee. J Comp Neurol 246:287–300.
Schmuker M, Yamagata N, Nawrot MP, Menzel R (2011) Parallel representation of stimulus identity and intensity in a dual pathway model inspired by the olfactory system of the honeybee. Front Neuroeng 4:17.
Seki Y, Rybak J, Wicher D, Sachse S, Hansson BS (2010) Physiological and morphological characterization of local interneurons in the Drosophila antennal lobe. J Neurophysiol 104:1007–1019.
Strauch M, Ditzen M, Galizia CG (2012) Keeping their distance? Odor response patterns along the concentration range. Front Syst Neurosci 6:71.
Tabor R, Yaksi E, Weislogel JM, Friedrich RW (2004) Processing of odor mixtures in the zebrafish olfactory bulb. J Neurosci 24:6611–6620.
Tanaka NK, Awasaki T, Shimada T, Ito K (2004) Integration of chemosensory pathways in the *Drosophila* second-order olfactory centers. Curr Biol 14:449–457.
Vosshall LB (2000) Olfaction in *Drosophila*. Curr Opin Neurobiol 10:498–503.
Wang JW, Wong AM, Flores J, Vosshall LB, Axel R (2003) Two-photon calcium imaging reveals an odor-evoked map of activity in the fly brain. Cell 112:271–282.
Witthöft W (1967) Absolute Anzahl und Verteilung der Zellen im Hirn der Honigbiene. Zeitschr Morphol Tiere 61:160–184.
Yamagata N, Schmuker M, Szyszka P, Mizunami M, Menzel R (2009) Differential odor processing in two olfactory pathways in the honeybee. Front Syst Neurosci 3:16.
Yamaguchi S, Wolf R, Desplan C, Heisenberg M (2008) Motion vision is independent of color in Drosophila. Proc Natl Acad Sci U S A 105:4910–4915.
Zwaka H, Munch D, Manz G, Menzel R, Rybak J (2016) The circuitry of olfactory projection neurons in the brain of the honeybee, *Apis mellifera*. Front Neuroanat 10:90.

(Received 31 July 2017, Accepted 12 January 2018)
(Available online 31 January 2018)